INTERNATIONAL JOURNAL FOR NUMERICAL METHODS IN FLUIDS
Int. J. Numer. Meth. Fluids 2000; **34**: 585–607

Numerical heat transfer in a cavity with a solar control coating deposited to a vertical semitransparent wall

G. Alvarez[a,*,1] and C. A. Estrada[b,2]

[a] *CENIDET-DGIT-SEP, AP 5-164, Cuernavaca, Morelos, Mexico*
[b] *Centro de Investigaciones en Energía—UNAM, AP 34, Temixco, Morelos, Mexico*

SUMMARY

A transient two-dimensional computational model of combined natural convection, conduction, and radiation in a cavity with an aspect ratio of one, containing air as a laminar and non-participating fluid, is presented. The cavity has two opaque adiabatic horizontal walls, one opaque isothermal vertical wall, and an opposite semitransparent wall, which consists of a 6-mm glass sheet with a solar control coating of SnS–Cu_xS facing the cavity. The semitransparent wall also exchanges heat by convection and radiation from its external surface to the surroundings and allows solar radiation pass through into the interior of the cavity. The momentum and energy equations in the transient state were solved by finite differences using the alternating direction implicit (ADI) technique. The transient conduction equation and the radiative energy flux boundary conditions are coupled to these equations. The results in this paper are limited to the following conditions: $10^4 \leq Gr \leq 10^6$, an isothermal vertical cold wall of 21°C, outside air temperatures in the range $30°C \leq T_0 \leq 40°C$ and incident solar radiation of AM2 (750 $W\,m^{-2}$) normal to the semitransparent wall. The model allows calculation of the redistribution of the absorbed component of solar radiation to the inside and outside of the cavity. The influences of the time step and mesh size were considered. Using arguments of energy balance in the cavity, it was found that the percentage difference was less than 4 per cent, showing a possible total numerical error less than this number. For $Gr = 10^6$ a wave appeared in the upper side of the cavity, suggesting the influence of the boundary walls over the air flow inside the cavity. A Nusselt number correlation as a function of the Rayleigh number is presented. Copyright © 2000 John Wiley & Sons, Ltd.

KEY WORDS: cavities; natural convection; radiation; solar control coating

1. INTRODUCTION

Over the last two decades, new technologies have been proposed and developed to control the thermal gains through the large windowpanes of tall buildings to reduce their energy

* Correspondence to: Mechanical Engineering Department, CENIDET-DGIT-SEP, AP 5-164, Cuernavaca, Morelos CP 62050, Mexico.
[1] E-mail: cenidet2@infosel.net.mx
[2] E-mail: gace@infosel.net.mx

Received February 1999
Revised May 1999

consumption. Solar control coatings developed by chemical deposition, which is still in progress, is part of this new technology. The solar control coatings are used in buildings at locations with warm climates to control, in a spectrally selective manner, the incidence of sunlight to the rooms, and thus to reduce the thermal gains inside the building. However, an important optical characteristic of this kind of material is its high absorptance in the solar spectrum, which increases the temperature of the solar control coating and glasses. This increment of the film and glass temperatures may cause additional thermal gains inside the room instead of reducing them.

Several models have been developed to get a better understanding of the thermal performance in a room. Natural convection in cavities heated differentially with adiabatic top and bottom walls has become the classical research problem that has been studied extensively by experimental, analytical, and numerical methods to get a better understanding of the governing processes [1–4]. Combined natural convection, conduction, and radiation in a cavity appears in the work of Larson [5]. He considered a cavity with radiation exchange between opaque walls and non-participating media with a high temperature source. Other authors [6,7], in studies considering the effects of long wave radiation, included participating and non-participating media in an insulated enclosure. Webb and Viskanta [8], in considering incident solar radiation, presented experimental and numerical steady state results of natural convective flow in a cavity with a semitransparent vertical wall and a participant media. Behnia *et al*. [9] presented the same case as before but with a non-participating media and no incident radiation. The studies presented by these authors mostly considered steady state conditions of combined convection and radiation, but a few of them considered a semitransparent wall and presented correlations between the Nusselt and the Rayleigh numbers. However, none of them considered the transient process of the combined heat transfer in a cavity with a solar control coating deposited onto a semitransparent wall, and hence there is no such correlation for this case.

In order to understand the thermal performance of a room with a glass window with solar control coating, a theoretical study of a transient two-dimensional model of a cavity with a semitransparent wall for low Grashof numbers is presented. This study considers normal incident solar radiation, conduction of energy through the semitransparent wall, radiative exchange between the walls and a radiatively non-participating fluid. The governing equations are solved numerically. Also, the correlation between Nusselt and Rayleigh numbers and the shading coefficient as a function of the ambient temperature are presented in this problem.

2. PHYSICAL MODEL

The two-dimensional air-filled cavity with an aspect ratio of one is shown in Figure 1. The airflow inside the cavity is considered to be laminar. The left face of the cavity is an isothermal opaque wall at 21°C; the right face is a semitransparent conductive wall with a SnS–Cu_xS solar control coating on it, where normal solar radiation flux is transmitted through it. The conduction heat transfer process in the semitransparent wall is considered as

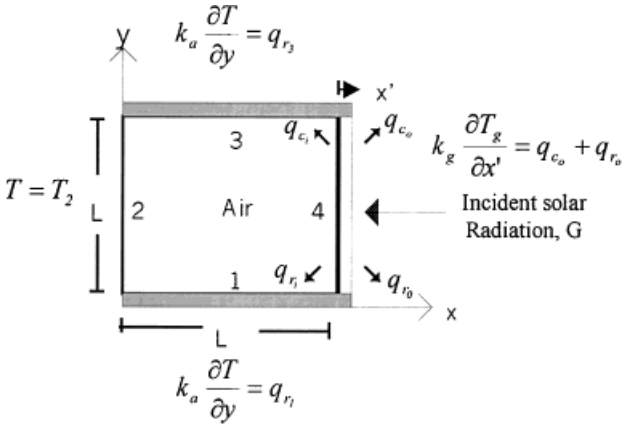

Figure 1. Physical model and the co-ordinate system.

one-dimensional. The two assumptions, the two-dimensional air filled cavity and the laminar air flow, are first approaches to solving the problem. The first assumption can be somewhat realistic if the cavity is thought of as a long cavity with its third dimension normal to the plane of the paper. The second assumption is for small cavities. Even though normal size rooms are for $Gr \geq 10^9$, small cavities could give a first approach to the thermal behavior of the cavity with solar control coatings on windows. The Boussinesq approximation is assumed in the governing equations. This approximation implies that, in the momentum equation, T is taken as the difference between $T_2 - T_H$, where T_2 is the temperature of the isothermal wall and T_H was chosen as the maximum temperature reached by the solar control coating of the semitransparent wall. The opaque and semitransparent walls are considered gray, diffuse reflectors, and emitters of radiation. It is well known that a glass reflects in a specular manner; however, inside an enclosure there are multiple reflections and the directionality of each reflection is lost considering the heat fluxes in the boundaries. The optical and thermophysical properties are considered constant. The glass transmittance and reflectance as a function of the solar incident angle are practically constant for angles less than 60°; although the solar control coating transmittance and reflectance do depend on the wavelength (in the visible region increases up to 40 per cent, but in the near infrared region remains constant and its value is less than 20 per cent), the optical properties considered here are the integrated spectrum values. The fluid inside the cavity is assumed to be radiatively non-participating for a low content of water vapor. The thickness of the glass is 6 mm, with a solar control coating of SnS–Cu_xS with negligible thickness (< 6 μm). The properties are given in Table I. The initial temperature is 21°C (294 K) and the incident solar radiation flux in the solar control semitransparent wall is assumed to be normal with a constant value of AM2 (750 W m^{-2}).

Table I. Optical and thermophysical properties of glass and SnS–Cu_xS solar control coating.

Glass (6 mm)	Glass (3 mm)	Film (SnS–Cu_xS)	Air
$\alpha_g = 0.14$	$\alpha_g = 0.06$	$A^*_{sol} = 0.64$	$k_a = 26.3 \times 10^{-3}$ W m^{-1} K
$\tau_g = 0.78$	$\tau_g = 0.86$	$T^*_{sol} = 0.15$	$\nu = 15.89 \times 10^{-6}$ m^2 s^{-1}
$\rho_g = 0.08$	$\rho_g = 0.08$	$R^*_{sol} = 0.16$	$C_{p_a} = 1.012$ kJ kg^{-1} K
$\varepsilon_g = 0.85$		$\varepsilon_f = 0.40$	$\text{Dens}_a = 1.204$ kg m^{-3}
$k_g = 1.12$ W m^{-1} K	$\text{Dens}_g = 2500$ kg m^{-3}	$C_{p_g} = 0.750$ kJ kg^{-1} K	

3. MATHEMATICAL MODEL

The governing equations are those of the conservation of mass, momentum, and energy equations for a square cavity with radiative exchange at the boundaries and conduction in the solar control semitransparent wall. As the streamfunction–vorticity formulation is used, the continuity equation is automatically satisfied and the pressure is eliminated as a solution variable. The equations are expressed in a dimensionless form as

$$\frac{\partial \zeta}{\partial \tau} + U\frac{\partial \zeta}{\partial X} + V\frac{\partial \zeta}{\partial Y} = \frac{1}{Gr^{1/2}}\left[\frac{\partial^2 \zeta}{\partial X^2} + \frac{\partial^2 \zeta}{\partial Y^2}\right] + \frac{T_H}{\Delta T}\frac{\partial \theta}{\partial X} \tag{1}$$

$$\frac{\partial^2 \psi}{\partial X^2} + \frac{\partial^2 \psi}{\partial Y^2} = -\zeta \tag{2}$$

$$\frac{\partial \theta}{\partial \tau} + U\frac{\partial \theta}{\partial X} + V\frac{\partial \theta}{\partial X} + V\frac{\partial \theta}{\partial Y} = \frac{1}{Pr\,Gr^{1/2}}\left[\frac{\partial^2 \theta}{\partial X^2} + \frac{\partial^2 \theta}{\partial Y^2}\right] \tag{3}$$

The velocities are related to the streamfunction by

$$U = \frac{\partial \psi}{\partial Y}, \qquad V = -\frac{\partial \psi}{\partial X} \tag{4}$$

The dimensionless variables were chosen according to Reference [10] as $X = x/L$, $Y = y/L$, $U = u/u_0$, $V = v/u_0$, $\zeta = \omega L/u_0$, $\psi = \Psi/u_0 L$, $\tau = tu_0/L$, $\theta = T/T_H$, where $u_0 = (g\beta\Delta TL)^{1/2}$.

The initial conditions in the cavity are those of a specified uniform temperature and a stagnant gas. The hydrodynamic boundary conditions are given in terms of the streamfunction as

$$\psi(0, Y, \tau) = \psi(1, Y, \tau) = \psi(X, 0, \tau) = \psi(X, 1, \tau) = 0 \tag{5}$$

The boundary conditions on vorticity are not known explicitly but will be determined by the Taylor series expansion of the streamfunction in the vicinity of the wall. The following energy

balances give the temperature boundary conditions on the top, bottom, and semitransparent wall:

Energy balance on the bottom insulated wall 1

$$q_{k_1} = q_{k_{a_1}} + q_{r_1} \quad \text{or} \quad \left.\frac{\partial\theta}{\partial Y}\right|_{Y=0} = N_r Q_{r_1}, \quad \text{with } N_r = \frac{\sigma T_H^3 L}{k_a} \quad \text{and} \quad Q_{r_1} = \frac{q_{r_1}}{\sigma T_H^4} \tag{6}$$

Boundary condition for the isothermal wall 2

$$T = T_2, \qquad \theta_2 = \frac{T_2}{T_H}, \qquad \theta = \theta_2 \tag{7}$$

Boundary condition for the insulated wall 3

$$\left.\frac{\partial\theta}{\partial Y}\right|_{Y=L} = N_r Q_3, \quad \text{with } N_r = \frac{\sigma T_H^3 L}{k_a} \quad \text{and} \quad Q_{r_3} = \frac{q_{r_3}}{\sigma T_H^4} \tag{8}$$

The temperature boundary condition for the vertical semitransparent wall 4 has had careful consideration. The conduction equation for this wall is coupled to the fluid energy equation by its interior boundary condition. Thus, the *conduction equation in dimensionless form of wall 4*

$$\frac{\partial\theta_4}{\partial\tau} = \frac{N_a}{N_L^2 Pr\sqrt{Gr}}\left[\frac{\partial^2\theta_4}{\partial X'^2} + \frac{dF'}{dX'}\right] \tag{9}$$

with $F' = N_{r_w} G' \exp[-s_g L_w(1 - X')]$.

With the following boundary conditions:

1. energy balance between the inside air and the solar control coating $q_{\text{absorbida}} = q_k - q_{k_a} + q_{r_4}$ in dimensionless form

$$\left.\frac{\partial\theta_g}{\partial X'}\right|_{X'=0} + \alpha_f \tau_g N_{r_w} G' - \frac{N_L}{N_k}\left.\frac{\partial\theta_a}{\partial X}\right|_{X=1} - N_{r_w} Q_{r_4} = 0 \tag{10}$$

2. energy balance between the glass and ambient air

$$\left.\frac{\partial\theta_g}{\partial X'}\right|_{X'=L_w} + N_h[\theta_g(L_w) - \theta_0] + N_{r_w}\varepsilon_g[\theta_g^4(L_w) - \theta_0^4] = 0 \tag{11}$$

with $N_h = L' h_\infty / k_g$.

The local Nusselt number in dimensionless form is given by

$$Nu_x = -\frac{1}{\theta_f - \theta_2}\frac{\partial\theta}{\partial X} \tag{12}$$

The dimensionless temperature of the vertical wall, opposite to the vertical semitransparent wall, is specified as $\theta(0, Y) = 0.84$, which corresponds to 21°C (294 K).

The terms Q_{r_1}, Q_{r_2}, Q_{r_3}, and Q_{r_4} are the dimensionless radiative fluxes inside the walls of the cavity given by the radiative transfer equations. For gray diffusive walls with an arbitrary temperature distribution, the configuration factors between any pair of elements of the boundary must be determined. The radiative heat flux along wall i is given by

$$q_{r_1} = J_1(x_1) - q_1(x_1) \tag{13}$$

with

$$J_1(x_1) = \varepsilon_1\sigma T_1^4 + \rho_1 q_1(x_1) \quad \text{and} \quad q_1(x_1) = \sum_{j=1}^{m}\int_{A_j} J_1(r_j)\,\mathrm{d}F_{1-j} \tag{14}$$

where $q_i(x_i)$ is the incoming radiative heat flux of the wall i and J_i is the radiosity. For each wall of the cavity, the configuration factors F_{i-j} for a square cavity are already given in Reference [10]. Thus, for the corresponding wall

$$J_1(x_1) = \varepsilon_1\sigma T_1^4(x_1) + \frac{\rho_1}{2}\left\{\int_0^L \frac{J_2(y_2)x_1x_2}{[x_1^2+y_2^2]^{3/2}}\,\mathrm{d}y_2 + \int_0^L \frac{J_3(x_3)H^2}{[H^2+(x_3-x_1)^2]^{3/2}}\,\mathrm{d}x_3 + \int_0^L \frac{J_4(y_4)(L-x_1)y_4}{[y_4^2+(L-x_1)^2]^{3/2}}\,\mathrm{d}y_4\right\} \tag{15}$$

$$J_2(y_2) = \varepsilon_2\sigma T_2^4(y_2) + \frac{\rho_2}{2}\left\{\int_0^L \frac{J_1(x_1)y_2x_1}{[y_2^2+x_1^2]^{3/2}}\,\mathrm{d}x_1 + \int_0^L \frac{J_3(x_3)(H-y_2)x_3}{[(H-y_2)^2+x_3^2]^{3/2}}\,\mathrm{d}x_3 + \int_0^L \frac{J_4(y_4)L^2}{[L^2+(y_4-y_2)^2]^{3/2}}\,\mathrm{d}y_4 + 2\tau_f\tau_g G\right\} \tag{16}$$

$$J_3(x_3) = \varepsilon_3\sigma T_3^4(x_3) + \frac{\rho_3}{2}\left\{\int_0^L \frac{J_1(x_1)H^2}{[H^2-(x_1-x_3)]^{3/2}}\,\mathrm{d}x_1 + \int_0^L \frac{J_2(y_2)x_3(H-y_2)}{[x_3^2+(H-y_2)^2]^{3/2}}\,\mathrm{d}y_2 + \int_0^L \frac{J_4(y_4)(H-y_4)(L-x_3)}{[(H-y_4)^2+(L-x_3)^2]^{3/2}}\,\mathrm{d}y_4\right\} \tag{17}$$

$$J_4(y_4) = \varepsilon_4 \sigma T_4^4(x_4) + \frac{\rho_4}{2}\left\{\int_0^L \frac{J_1(x_1)y_4(L-x_1)}{[y_4^2+(L-x_1)]^{3/2}}\,\mathrm{d}x_1 + \int_0^L \frac{J_2(y_2)L^2}{[L^2+(y_2-y_4)^2]^{3/2}}\,\mathrm{d}y_2 + \int_0^L \frac{J_3(x_3)(H-y_4)(L-x_3)}{[(H-y_4)^2+(L-x_3)^2]^{3/2}}\,\mathrm{d}x_3\right\} \tag{18}$$

In solving the radiosity equations, dimensional values are used in the calculation of the radiative fluxes on the boundaries, then the result is non-dimensionalized.

4. METHOD OF SOLUTION

Equations (1)–(4), the conduction equation (9) along with the radiative flux equations (13)–(18), and their initial and boundary conditions (5)–(11) define the problem completely. The equations are all coupled through the boundary conditions and/or the variables. Forward time and central space differences approximated the derivatives of the partial differential equations (1) and (3). The alternating direction implicit (ADI) finite difference technique was used. The streamline equation (2) was solved by the method of Paceman and Rachford [11]. The conduction differential equation was solved numerically by using an explicit finite difference formulation. The radiosity equations were solved by the method of successive approximation. The integrals were evaluated by the Simpson's rule. The net radiative heat fluxes were calculated from the radiative net heat flux equation (13).

The temperature boundary condition of the interior semitransparent wall must have careful consideration. The discretized couple boundary condition of the interior side of the semitransparent wall with the solar control coating gives

$$B_1\theta_{\mathrm{f}}^k + B_2 Q_{\mathrm{r}_4} - \theta_{\mathrm{w}_2}^k + B_{3_j} = 0 \tag{19}$$

with

$$B_1 = 1 - \frac{3N_L\Delta X'}{2\Delta X N_k},$$

$$B_2 = N_{\mathrm{r}_{\mathrm{w}}}\Delta X' \quad \text{and} \quad B_{3_j} = -\Delta X'\alpha_{\mathrm{f}}\tau_{\mathrm{g}}N_{\mathrm{r}_{\mathrm{w}}}G' - \frac{N_L}{N_k}\frac{\Delta X'}{2\Delta X}[4\theta_{M,j}^k - \theta_{M-1,j}^k]$$

where θ_{f}^k is the solar control coating temperature, Q_{r_4} the net radiative heat flux of the interior side of the semitransparent wall and $\theta_{M,j}^k$ and $\theta_{M-1,j}^k$ are the air temperatures close to the solar control coating of the semitransparent wall corresponding to the co-ordinate $y = j\cdot\Delta y$. The net radiative heat flux Q_{r_4} is calculated using Equation (13).

For the external side of the semitransparent wall

$$C_1\theta_{\mathrm{w}_{N+1}}^k + C_2\theta_{\mathrm{w}}^{4k} - \theta_{\mathrm{w}_N}^k + C_3 = 0 \tag{20}$$

with

$$C_1 = 1 + N_h \Delta X', \qquad C_2 = N_{r_w} \varepsilon_g \Delta X' \quad \text{and} \quad C_3 = -N_h \Delta X' \theta_0 - N_{r_w} \varepsilon_g \Delta X' \theta_0^4$$

The boundary values of the vorticity were calculated using the Taylor series expansion of the streamfunction; using the boundary conditions on ψ and from the streamfunction equation (2), the boundary conditions on ζ were calculated as

$$\zeta_{1,j}^{k+1} = -\frac{2\psi_{2,j}}{2\Delta Y^2}, \qquad \zeta_{M+1,j}^{k+1} = -\frac{2\psi_{M,j}}{2\Delta X^2}, \qquad \zeta_{i,1}^{k+1} = -\frac{2\psi_{i,2}}{2\Delta Y^2}, \qquad \zeta_{i,j}^{k+1} = -\frac{2\psi_{i,j}}{2\Delta Y^2} \tag{21}$$

The solution procedure went in the following order. Knowing the initial and boundary values of temperature and velocity, the radiosity equations (15)–(18) were calculated, then the radiative net heat flux of the walls, Equation (13), was computed. As solar energy radiation strikes the glass and the solar control coating, the energy conduction equation (9) for the glass wall and their boundary conditions (19) and (20) were solved to update the temperature distribution of the wall. The normal temperature gradients in the upper and lower wall were calculated from Equations (6) and (8); the partial differential equation (3) was solved to obtain the inside air temperature patterns. Then, the vorticity–transport equation (1) and the streamfunction equation (2) were solved. After that, the boundary values of the vorticity equation (21) were updated, then the velocity field from Equation (4) was calculated. The procedure was repeated until a steady state was reached.

5. RESULTS

The solar radiation, the external convective heat transfer coefficient, the ambient temperature, the radiative properties and the cavity size affect the flow and thermal fields inside the cavity. Figure 2 shows the maximum temperature T_H reached by the solar control coating of the semitransparent wall. The time at which the film temperature reached their maximum value was 0.5 ($\tau = 5$), afterwards T_H remains constant. Thus, the Grashof number is assumed constant during the whole numerical process.

The parameter values used here were for a square cavity containing air, as a laminar flow, for $Gr = 10^4$, 10^5, and 10^6, with an ambient exterior temperature of 35°C, an external convective heat transfer of 6.2 W m^{-2} °C and a cold vertical wall of 21°C. All the surface walls were assumed to have an emittance of 0.9 except for the semitransparent wall, which has an inside film emittance of 0.4 and an exterior glass emittance of 0.85. Table II shows the parameter values used in the simulation.

To determine the time step, grid size, and convergence criteria several numerical experiments were tested on a WS HP730. For Gr of 10^4, 10^5, and 10^6, a number of mesh sizes were employed to check the convergence of the numerical results. Figures 3 and 4 show the dimensionless temperature as a function of X for $Y = 0.5$ for Gr of 10^4 and 10^5 for uniform mesh sizes of $\Delta X = \Delta Y$ of 11×11, 21×21, and 31×31 and $\Delta\tau$ of 0.002, 0.001, and 0.0005 for

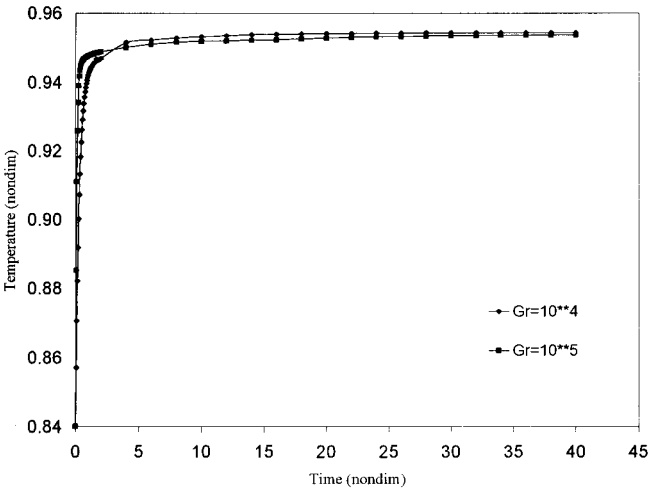

Figure 2. Temperature history of the solar control coating for $Gr = 10^4$ and 10^5.

Table II. Typical values of the parameter values used in the simulation.

$Gr = 10^4$–10^6	$N_k = 53.23$	$N_{r_g} = 0.0104$
$Pr = 0.73$	$N_\alpha = 0.0346$	$L = 0.0124$–0.058
$G' = 0.8815$	$N_h = 0.1313$	$u_0 = 0.0163$–0.0745
$T_H = 350$ K	$N_r = 1.151$–5.38	$\varepsilon_1 = \varepsilon_2 = \varepsilon_3 = 0.9$
$L' = 0.006$ m	$N_L = 0.103$–0.587	$\varepsilon_4 = \varepsilon_f = 0.4$

dimensionless time of $\tau = 6$ and 26. For Gr of 10^4 and 10^5, 31×31 nodal points and a time increment of 0.001 were adequate in terms of accuracy and computed economy. For $Gr = 10^6$, a mesh of 51×51 and a time increment of 0.0005 were satisfactory, but the computer time increases appreciably up to 15:36 h. Also, to validate the model, the computer program was structured in such a way that the problem can be reduced to neglect radiation and conduction through the semitransparent wall for comparison with the classical problem of natural convection in a cavity [12]. Table III shows this comparison. The values of the isotherms and the streamlines are in good agreement, presenting some differences at the corners of the cavity. These differences could be due to the procedure of curve fitting.

To examine the effects of the use of the solar control coating on the semitransparent wall and the radiative exchange between the walls, three cases were considered. *Case A:* the classical case of natural convection in a cavity with opaque vertical isothermal walls at different temperatures taken as reference case. *Case B:* the combined problem of natural convection, conduction, and radiation in a cavity with a glass + solar control coating. *Case C:* the same as case B except that the semitransparent wall is a clear glass. The semitransparent wall for both cases is located on the right side of the cavity.

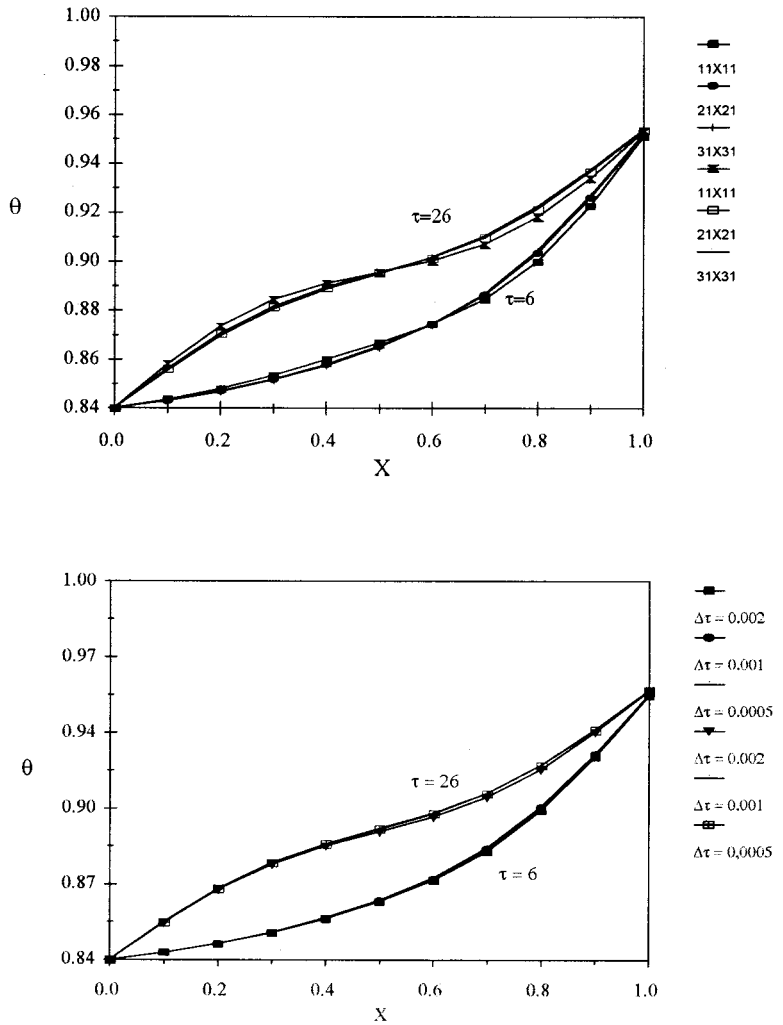

Figure 3. Temperature distribution as a function of X for $Y = 0.5$ for $Gr = 10^4$ for grid sizes of 11×11, 21×21, 31×31 and time increments of 0.002, 0.001, 0.0005 for $\tau = 6$ and 26.

Figure 5(a) and (b) shows a comparison of the transient isothermal and streamline plots for cases A and B for $Gr = 10^4$ and $\tau = 6$, 12, and 30. The semitransparent wall temperature (located on the right side) increases very rapidly due to the absorbed solar radiation by the solar control coating and the glass. For $\tau = 5$, the mean temperature of the film reaches 0.955 (61.1°C). This maximum value was chosen for the hot wall of case A. In case B, the isotherms compared with case A are less curved, indicating the influence of the radiative exchange. In the streamline figures, the fluid circulates in a counterclockwise direction. The flow patterns are

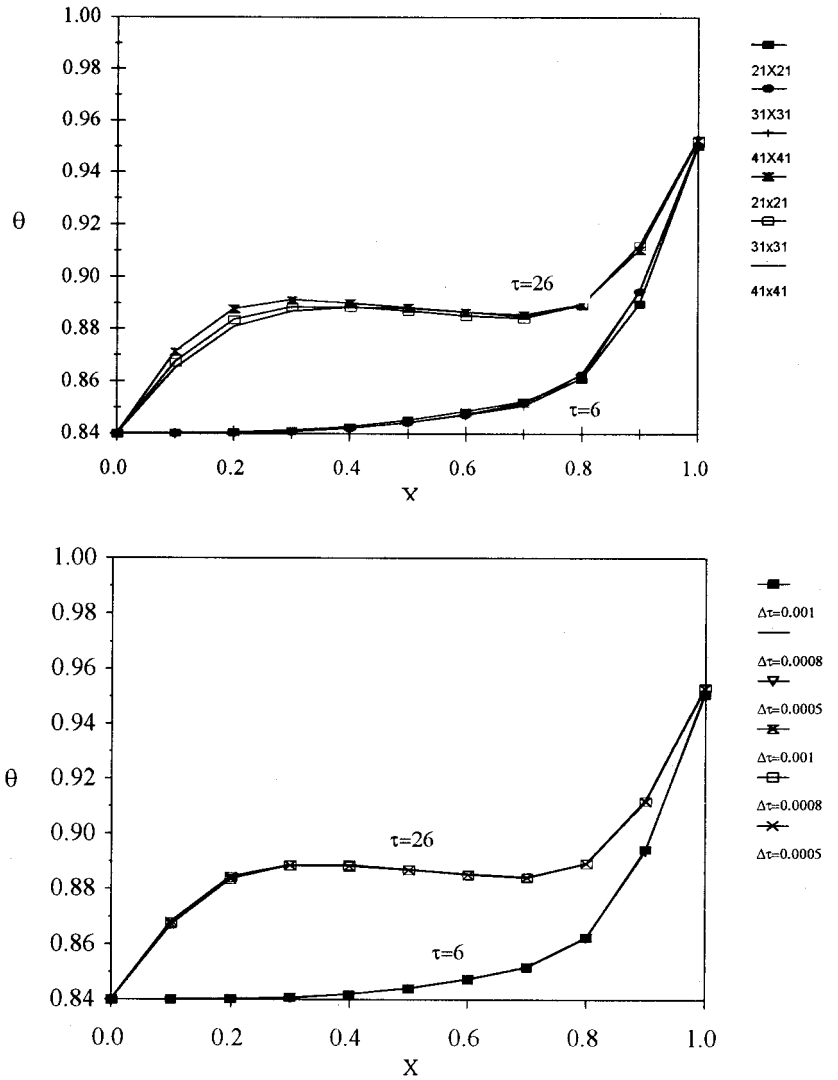

Figure 4. Temperature distribution as a function of X for $Y = 0.5$ for $Gr = 10^5$ for grid sizes of 11×11, 21×21, 31×31 and time increments of 0.002, 0.001, 0.0005 for $\tau = 6$ and 26.

very similar, but in case A, the fluid is moving faster than in case B, as indicated by the density of the streamlines. This is because, in case B, there are radiative exchanges between the walls, and thus the amount of energy transferred to the inside of the cavity is divided in two terms, convective and radiative; meanwhile, in case A, it is just convective energy.

Table III. Comparison between the natural convection results given by Wilkes and Churchill [12] and the actual model.

X	Y	Wilkes and Church [12], θ	Actual model, θ	%Dif.	X	Y	Wilkes and Church [12], ψ	Actual model, ψ	%Dif.
0.1	0.2	−0.75	−0.75	0.00	0.5	0.5	8.00	8.00	0.01
0.2	0.4	−0.50	−0.50	0.00	0.3	0.5	6.00	6.09	1.60
0.1	0.6	−0.50	−0.50	0.00	0.7	0.5	6.00	6.09	1.60
0.5	0.1	−0.50	−0.50	0.00	0.7	0.8	4.00	3.85	3.75
0.2	0.8	−0.25	−0.26	2.80	0.2	0.5	4.00	3.85	3.75
0.7	0.1	−0.25	−0.25	0.00	0.8	0.5	4.00	3.85	3.75
0.4	0.8	0.00	0.00	0.00	0.8	0.1	2.00	1.95	2.50
0.5	0.5	0.00	0.00	0.00	0.2	0.9	2.00	1.95	2.50
0.6	0.2	0.00	0.00	0.00	0.4	0.1	2.00	2.06	3.00
0.3	0.9	0.25	0.25	0.00	0.6	0.9	2.00	2.06	3.00
0.5	0.9	0.50	0.50	0.00	0.1	0.2	1.00	0.96	4.00
0.9	0.4	0.50	0.50	0.00	0.9	0.1	1.00	0.91	9.00
0.9	0.8	0.75	0.75	0.00	0.9	0.8	1.00	0.96	4.00

Figure 6(a) and (b) shows a comparison of the transient isotherms and streamlines hysterics for Gr of 10^5 and $\tau = 6$, 12, 20, and 30 for cases B and C. Although the shape of the isotherms looks similar, there are differences. The isotherms are less curved in case C than in case B, indicating that the convection regime is more pronounced in case B. That happens because part of the energy that goes through the glass + film is absorbed ($\alpha = 0.61$), increasing the temperature of the coating and glass and the heat absorbed is transferred to the fluid. The clear glass absorbs less energy ($\alpha = 0.14$), and thus transfers less energy by conduction to the fluid. The isotherms in the upper side are less curved in case C compared with case B, indicating that the diffusion is slower towards the core of the cavity. Looking at the streamlines, the effect of convection is more pronounced in case B compared with case C, which is very reasonable because the inside semitransparent wall temperature is higher, $\theta = 0.954$ (60.8°C), for case B than for case C, $\theta = 0.889$ (38.1°C).

Figure 7(a) and (b) is similar to Figure 6(a) and (b) but for Gr of 10^6. As the Grashof number increases, temperature gradients become more severe near the vertical walls and some stratification is presented at the center of the cavity. For $\tau = 6$, the isotherms of case C are less curved than in case B, indicating also that in case C convection is less significant than case B. At later times, $\tau = 30$ and 60, the isotherms in the core region are practically horizontal, indicating a temperature stratification. Looking at the streamlines, one vortex is presented in most of the times except for case B, $\tau = 30$ and 60, where two vortices are present. In both cases, the vortices are closer to the walls. The boundary layers adjacent to the walls are thin and fast compared with the ones of Figure 6. In case B, $\tau = 6$, the flow spreads out from the thin layer in the vertical wall and turns over, it starts to separate from the wall and then reattached to it. For case C, at the same time, this effect is not shown yet. At later times the effect is more pronounced, even for the two cases. This turn over effect has been already reported in natural convection cavities but for greater Grashof numbers [1,3,4] and not in combined natural convection and radiation.

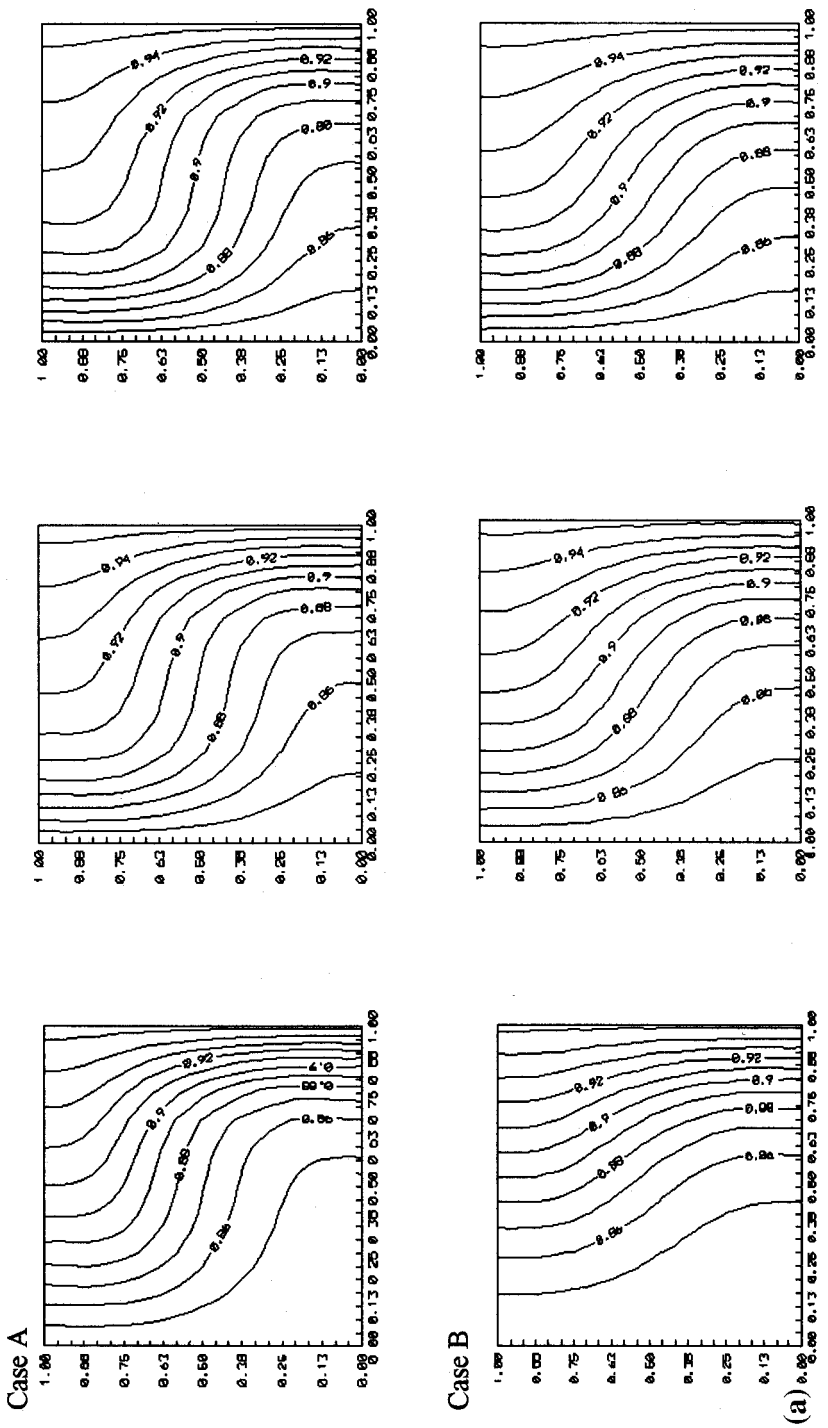

Figure 5. Isotherm (a) and streamline (b) histories for cases A and B, $Gr = 10^4$ and $\tau = 6$, 12, and 20, from left to right. For isotherms, minimum value of isoline 0.85, maximum value 0.95, increment 1. For streamlines: Case A, minimum value 0.001, maximum value 0.051, increment 2; Case B, minimum value 0.001, maximum value 0.031, increment 2.

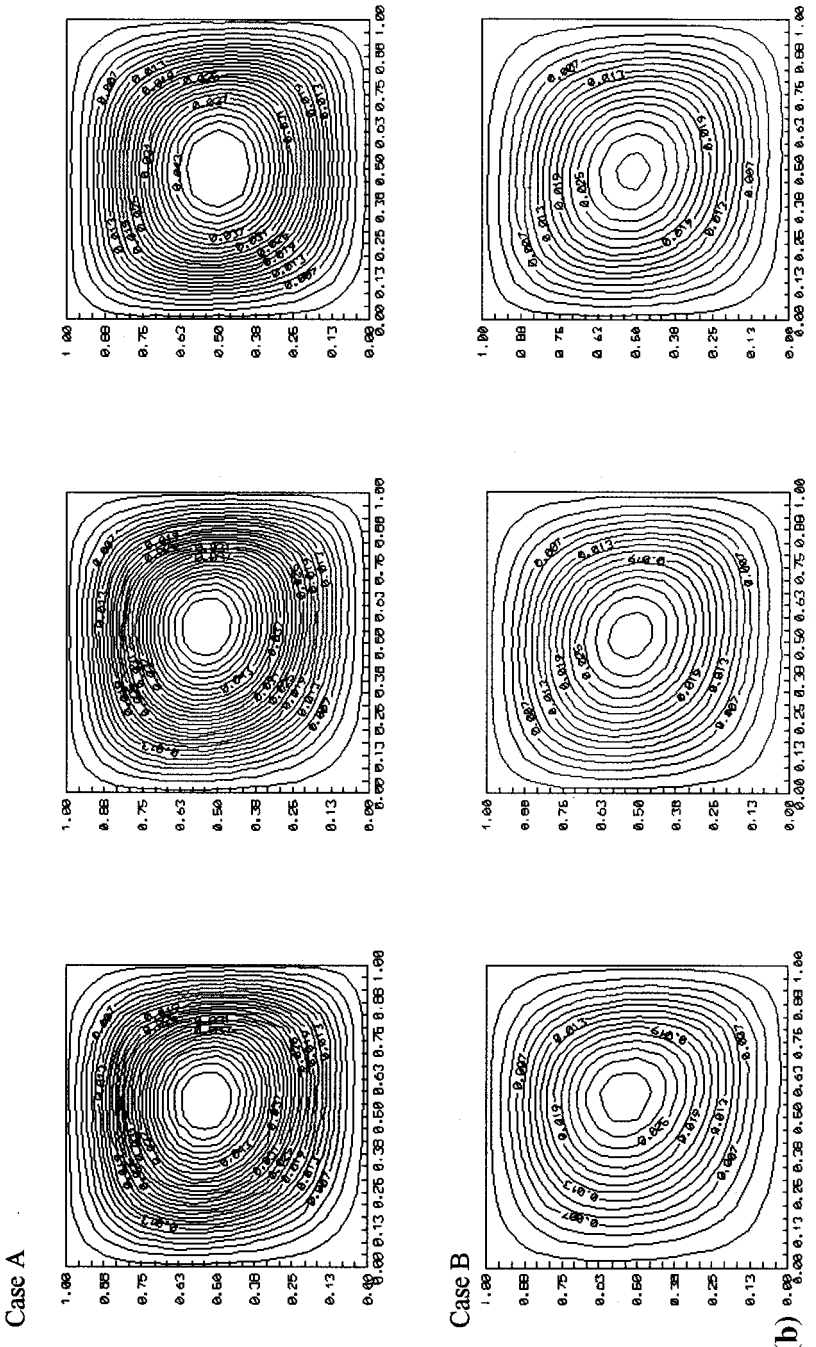

Figure 5 (*Continued*)

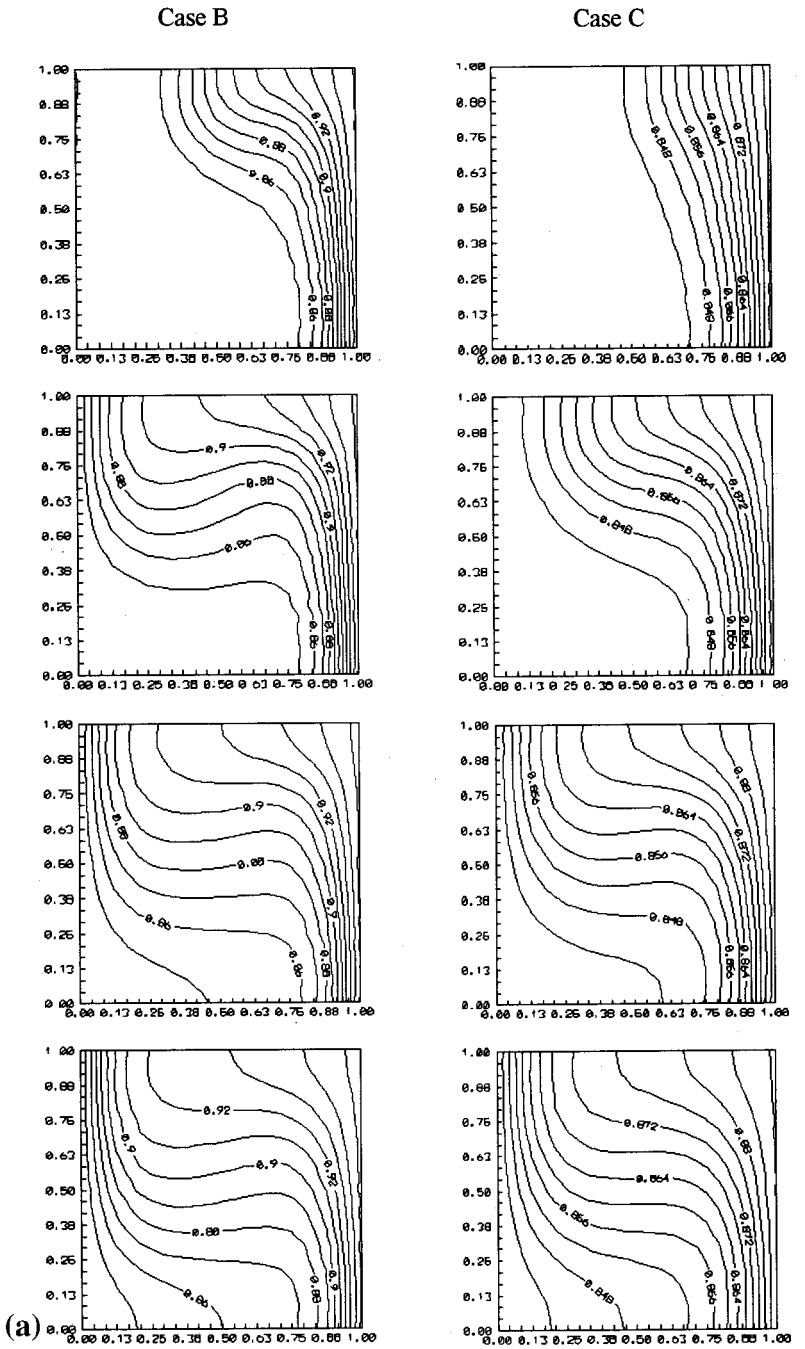

Figure 6. Isotherm (a) and streamline (b) histories for cases B and C, $Gr = 10^5$ and $\tau = 6$, 12, 20, and 40 from left to right. (a) Case B, minimum value 0.85, maximum value 0.95, increment 1; Case C, minimum value 0.84, maximum value 0.96, increment 0.04. (b) Case B, minimum value 0.001, maximum value 0.029, increment 2; Case C, minimum value 0.001, maximum value 0.021, increment 2.

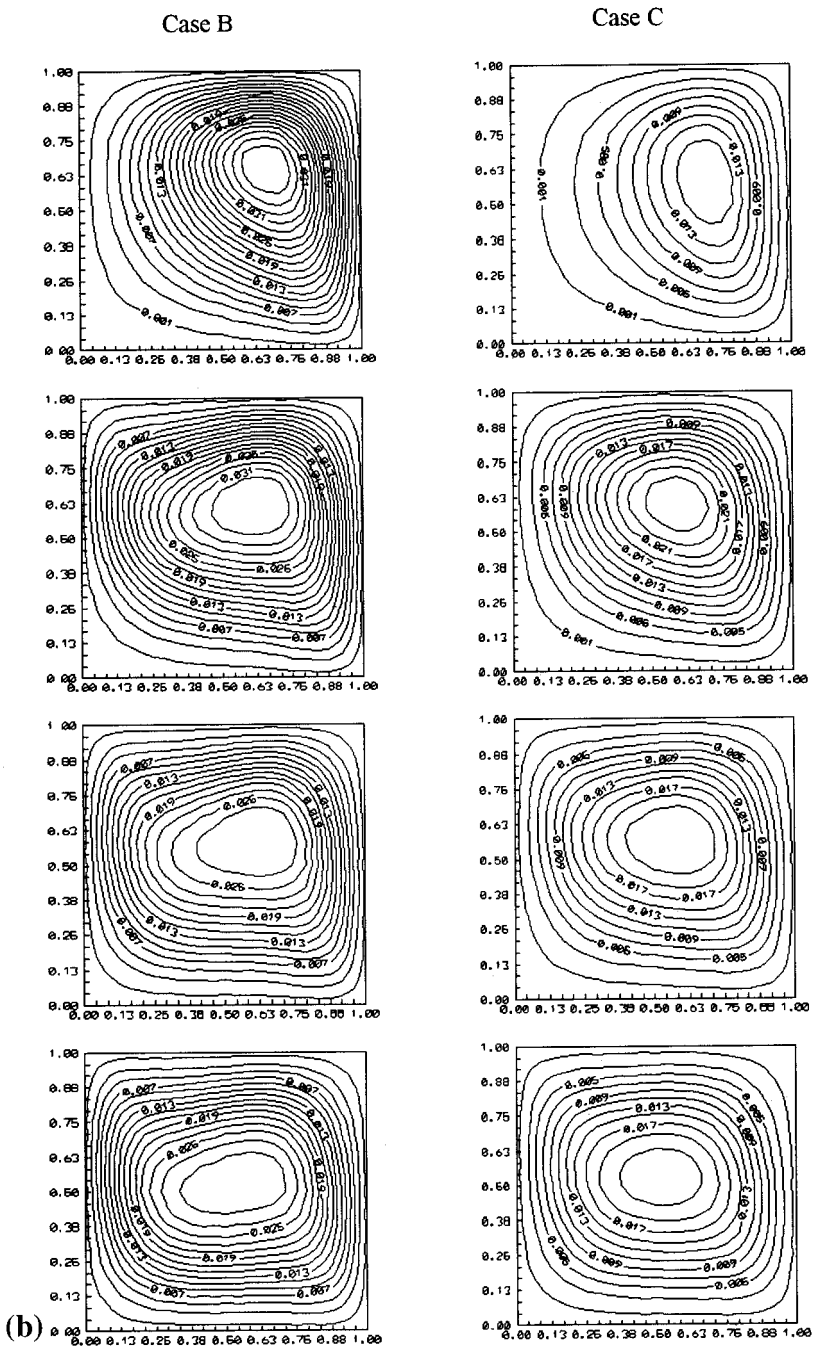

Figure 6 (*Continued*)

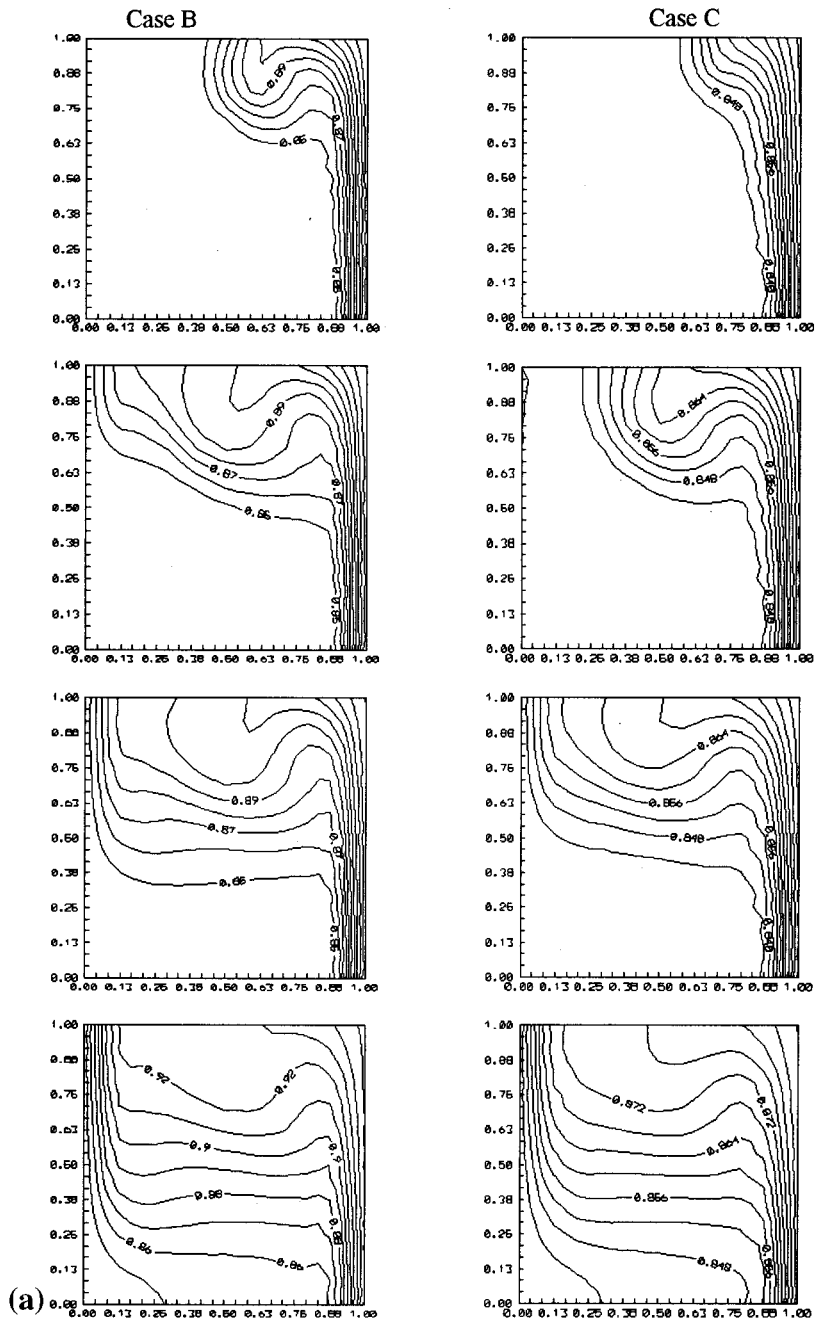

Figure 7. Isotherm (a) and streamline (b) histories for cases B and C, $Gr = 10^6$ and $\tau = 6$, 12, 30, and 60 from left to right. (a) Case B, minimum value 0.85, maximum value 0.95, increment 1. Case C, minimum value 0.840, maximum value 0.884, increment 0.004; (b) Case B, minimum value 0.001, maximum value 0.018, increment 2; Case C, minimum value 0.001, maximum value 0.013, increment 1.

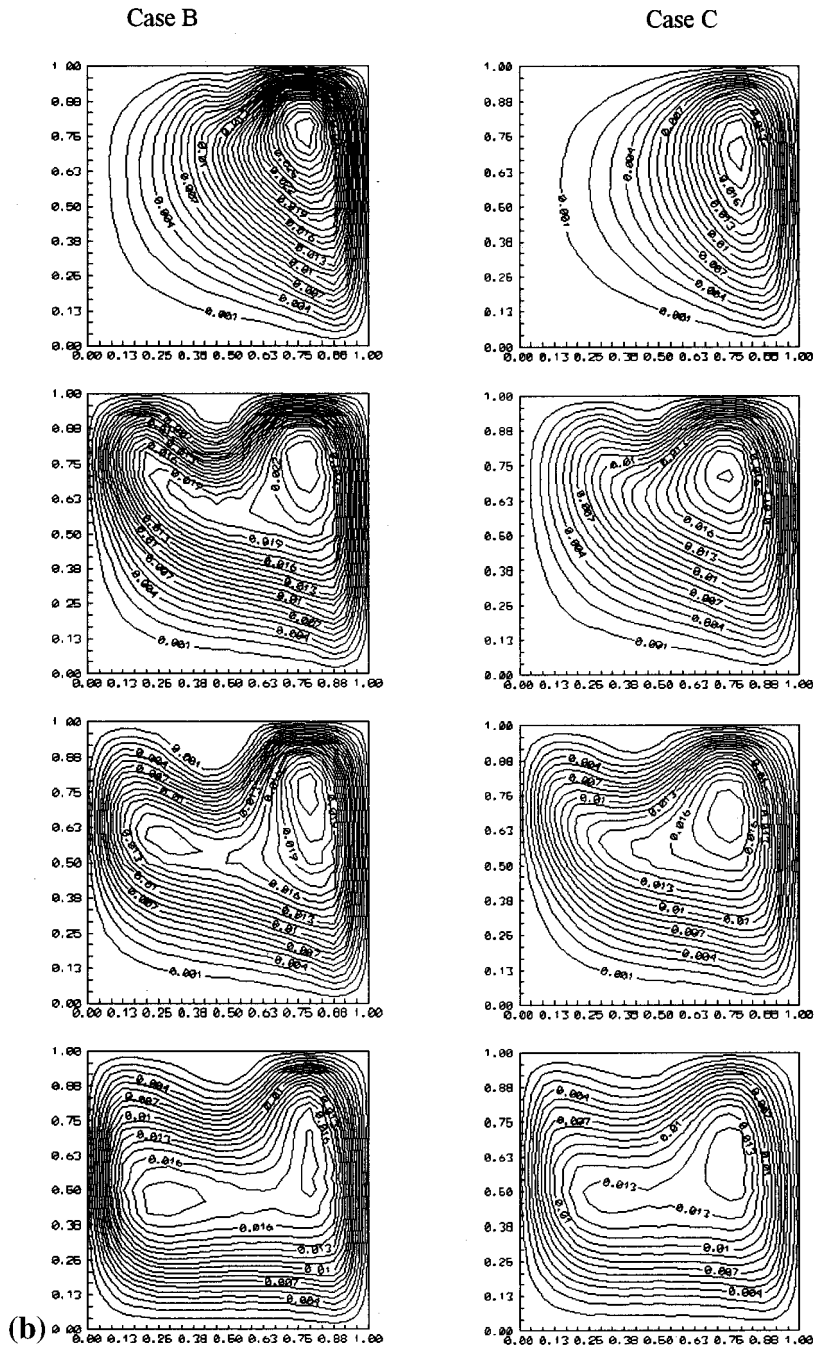

Figure 7 (*Continued*)

Figure 8 shows the vertical components of the velocity for cases A, B, and C for $Gr = 10^5$ and 10^6. From these figures we can appreciate that if you increase the Grashof number, the maximum of the vertical component of the velocity moves towards the vertical walls. Also, the difference in velocities for cases A, B, and C is appreciated, as well as the stratification of the fluid at the center.

A correlation for the average Nusselt number for the steady state were derived using least-square linear regression for $1 \times 10^4 \leq Gr \leq 5 \times 10^6$ and $Pr = 0.73$. The correlation is

$$\overline{Nu}_c = 0.0643(Ra)^{0.355} \quad \text{for } 7.3 \times 10^3 \leq Ra \leq 3.6 \times 10^6$$

To observe the contribution of radiation in this kind of problem, Behnia *et al.* [9] introduced a definition of a Nusselt number for radiation as $Nu_r = (q_{rad}/q_c) \cdot Nu_c$; thus giving the total Nusselt number as $Nu_T = Nu_c + Nu_r = (q_{rad}/q_c) \cdot Nu_c$. Using this, Figure 9 shows the variation of the convective and the radiative Nusselt number versus the Rayleigh number. The Nu_r increases slightly (almost constant) with the Ra number. This is due to the low range of temperatures considered.

In calculating the heat balance, Table IV shows the net heat flux going to the inside and outside of the cavity as well as the heat balance of the cavity for four different ambient temperatures. These percentage differences might indicate that the numerical error is around 4 per cent.

The shading coefficient (SC) is a standard parameter used in the glazing industry and measures the thermal heat gain efficiency through a glass window. It represents the ratio of the heat that goes to the interior of the cavity through the semitransparent wall to that for a clear 3-mm glass (case B with 3-mm glass) and can be expressed for the system glass + film as

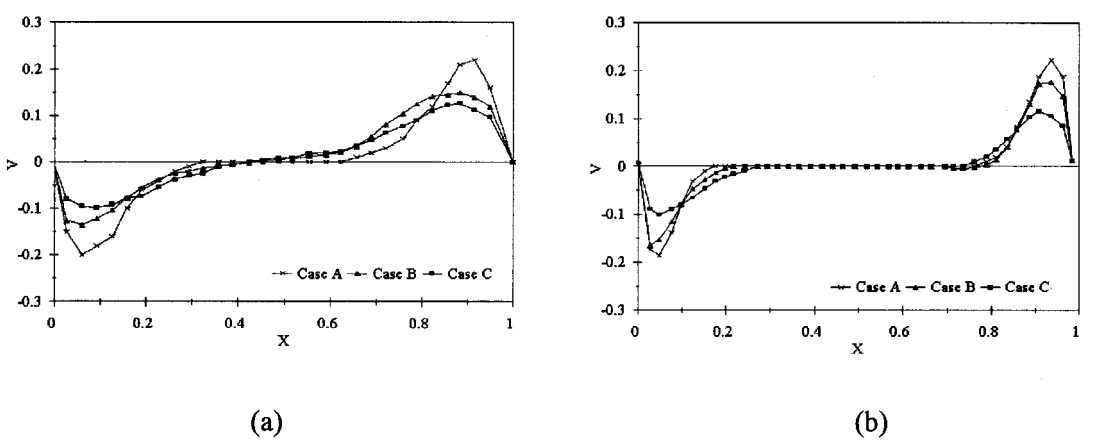

Figure 8. Steady state vertical velocity components for (a) $Gr = 10^5$ and (b) $Gr = 10^6$ for cases A, B, and C.

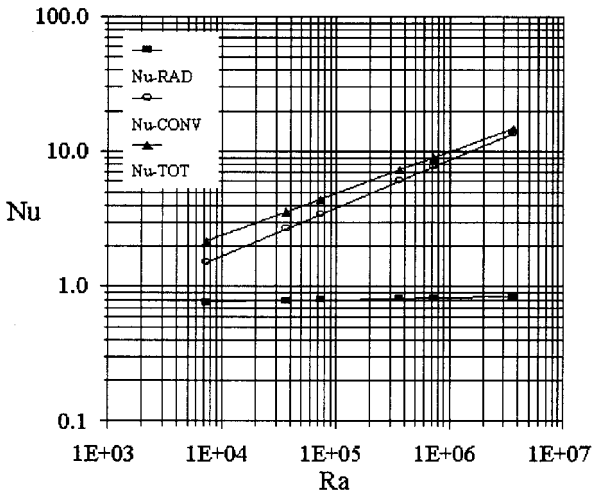

Figure 9. Convective, radiative, and total Nusselt number versus Rayleigh number.

Table IV. Net heat flows to the interior and exterior for the cavity with glass + solar control coating and clear glass for different ambient temperatures T_0 for $Gr = 10^5$.

T_0, °C	Q_{int} (case B), W m^{-2}	Q_{int} (case C), W m^{-2}	Q_{ext} (case B), W m^{-2}	Q_{ext} (case C), W m^{-2}	Q_{tot} (case B), W m^{-2}	Q_{tot} (case C), W m^{-2}	G, W m^{-2}	Dif.% Q_{tot} (case B)	Dif.% Q_{tot} (case C)
30	266.96	615.69	453.13	112.68	720.09	728.37	750	3.99	2.88
35	283.56	628.55	442.97	98.06	726.53	726.61	750	3.13	3.12
40	300.72	641.11	434.31	82.89	735.03	724.00	750	2.00	3.47
45	318.58	654.81	424.29	67.08	742.87	721.89	750	0.95	3.75

$$\mathrm{SC} = \frac{[q_i(T_0) + \tau G]_{\text{glass + film}}}{[q_i(T_0) + \tau G]_{\text{3-mm clear glass}}} \tag{24}$$

Figure 10 shows the curves for the SC versus ambient temperature. The upper curve is for a cavity with 6-mm thick clear glass and the lower curve for a cavity with a 6-mm thick glass with a solar control coating. It is observed that, for an ambient temperature of 35°C, the SC for the cavity using the solar control coating was 0.42, and 0.92 for the cavity with clear glass, indicating that, from the 100 per cent of energy that would go through a 3-mm thick clear glass, only 42 per cent goes through because of the use of a 6-mm thick glass with a solar control coating on it. If a clear glass of 6 mm is used, the heat gain to the inside of the cavity would be 92 per cent. This result demonstrates the advantage of the solar control coating used in windows.

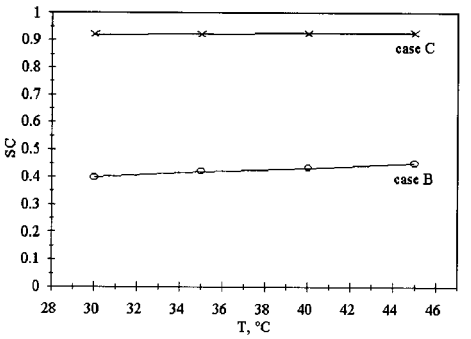

Figure 10. SC versus ambient temperature for cases B and C in steady state and $Gr = 10^5$.

6. CONCLUSIONS

A transient two-dimensional mathematical model of a combined natural convection, conduction, and radiation in a square cavity containing air as a laminar and non-participating fluid has been presented. One wall of the cavity was considered to be semitransparent with a solar control coating on it. The following conditions were used for the modeling: initial temperature of 21°C, normal incident AM2 solar radiation (750 $W\,m^{-2}$ °C) and ambient temperature T_0 of 35°C for $10^4 \leq Gr \leq 10^6$ and $30°C \leq T_0 \leq 45°C$ for $Gr = 10^5$. Two comparisons were presented: (1) between the classical problem of natural convection in a cavity with isothermal opaque walls and a vertical semitransparent wall with a solar control coating, and (2) between a cavity with a vertical semitransparent wall with a solar control coating and without a solar control coating. From the first comparison, an influence of the radiative exchange on the flow and temperature patterns was observed. A decrease in the convective regime was detected. From the second comparison, a similar pattern was observed qualitatively but not quantitatively. The movement of the flow is slower in the cavity with the clear glass. For $Gr = 10^6$ and for all the cases, a wave effect appears on the upper side of the cavity.

A correlation between the convective and radiative Nusselt number as a function of the Rayleigh number for the cavity with SnS–Cu_xS solar control coating was developed. This is one of the most important results of this study. However, from the industry point of view, the shading coefficient is a more important parameter, which is presented as a function of the ambient temperature. In general, these results indicate that according to the one-dimensional model reported by Estrada *et al.* [13], even though the glass and the solar control coating are warmer than the clear glass, the energy transferred by conduction and solar energy transmitted through the glass/solar control coating system is lower than that in the case of a system that uses clear glass. The difference was about 50.2 per cent, suggesting a strong advantage, from the thermal point of view, for using the solar control coating on glass windows.

APPENDIX A. NOMENCLATURE

A^*	solar absorptance, %
C_p	specific heat
g	gravity, m s^{-2}
G	incident solar radiation, W m^{-2}
G'	dimensionless incident solar radiation; $G/\sigma T_H^4$
Gr	Grashof number; $g\beta\Delta TL^3/v^2$
h_∞	heat transfer coefficient, W m^{-2}, K
H	height of cavity, m
J_i	radiosity of wall y
k	conductivity, W m^{-1} K
L	width of cavity, m
L'	thickness of glass, m
N_α	dimensionless parameter; α_g/α
N_h	dimensionless parameter; hL'/k_g
N_k	dimensionless parameter; k_w/k_a
N_L	dimensionless parameter; L'/L
N_r	radiative number; $\sigma T_H^3 L/k_a$
Nu	Nusselt number; hL/k_a
Pr	Prandtl number; v/α
q_i	incident energy on wall i
q_c	convective heat transfer
q_k	heat conduction, W m^{-2}
q_{r_i}	net radiation of wall i
Ra	Rayleigh number; $Pr\,Gr$
R^*_{sol}	integrated reflectance, %
s_g	extinction coefficient of glass, m^{-1}
SC	shading coefficient
t	time, s
T	temperature, K
T^*_{sol}	integrated transmittance, %
T_H	maximum film coating temperature, K
u_0	reference velocity, m s^{-1}
u, v	velocity components, m s^{-1}
U, V	dimensionless velocity; u/u_0
x, y, x'	co-ordinate axis
X, Y	dimensionless co-ordinate axis

Greek letters

α	air diffusivity, m^2 s^{-1}
α_g	glass absorptance
β	thermal expansion coefficient, K^{-1}

ε	emittance
ν	kinematic viscosity, $m^2\,s^{-1}$
ρ_i	reflectance of wall i
θ	dimensionless temperature, T/T_H
σ	Stefan–Boltzman constant, $W\,m^{-2}\,K^{-4}$
τ_g	glass transmissivity
τ	dimensionless time; tu_0/L
ω	vorticity
ψ	streamlines
ζ	dimensionless vorticity
Ψ	dimensionless streamlines

Indices

i	incident energy on wall i
a	air
r_i	net radiation on wall i
f,4	film
H	maximum temperature
k	conduction
g	glass

REFERENCES

1. Ivey GN. Experiments on transient natural convection in a cavity. *Journal of Fluid Mechanics* 1984; **144**: 389–401.
2. Ostrach S. Natural convection in enclosures. *Transactions of ASME*, *Journal of Heat transfer* 1988; **110**: 1175–1190.
3. Paolucci S, Chenoweth DR. Natural convection in shallow enclosures with differentially heated endwalls. *Transactions of ASME*, *Journal of Heat Transfer* 1988; **110**: 625–634.
4. Roache PJ. *Computational Fluid Dynamics*. Hermosa Publishers: Albuquerque, NM, 1982.
5. Larson DW. Analytical study of heat transfer in an enclosure. PhD thesis, Purdue University, 1972.
6. Chang LC, Yang KT, Lloyd JR. Radiation–natural convection interactions in two-dimensional complex enclosures. *Journal of Heat Transfer* 1983; **105**: 89–95.
7. Lauriat G. Combined radiation convection in gray fluids enclosed in vertical cavities. *Journal of Heat Transfer* 1982; **104**: 609–615.
8. Webb BW, Viskanta R. Radiation induced buoyancy driven flow in rectangular enclosures: experiment and analysis. *Journal of Heat Transfer* 1987; **109**: 427–433.
9. Behnia M, Rizes JA, de Vahl Davis G. Combined radiation and natural convection in a cavity with a semitransparent wall and containing a non-participant fluid. *International Journal for Numerical Methods in Fluids* 1990; **10**: 305–325.
10. Larson DW, Viskanta R. Transient combined laminar free convection and radiation in a rectangular enclosure. *Journal of Fluid Mechanics* 1976; **78**: 65–85.
11. Ravi MR, Henkes RAW, Hoogendoon J. On the high Rayleigh number structure of steady laminar natural convection flow in square enclosure. *Journal of Fluid Mechanics* 1994; **262**: 325–351.